Supporting Information

Janus Electrocatalysts Containing MOF-derived Carbon Networks and NiFe-LDH Nanoplates for Rechargeable Zn-air Batteries

Yuhong Qian,[†] Tao An,[‡] Erik Sarnello,[¶] Zhaolin Liu,[‡] Tao Li[¶, §] and Dan Zhao*[, †]

[†] *Department of Chemical and Biomolecular Engineering, National University of Singapore, 4 Engineering Drive 4, Singapore 117585*

[‡] *Institute of Materials Research and Engineering (IMRE), A*STAR (Agency for Science, Technology and Research), Innovis, 2 Fusionopolis Way, Singapore 138634*

[¶] *Department of Chemistry and Biochemistry, Northern Illinois University, DeKalb, Illinois 60115, United States*

[§] *X-ray Science Division, Argonne National Laboratory, Lemont, Illinois 60439, United States*

*E-mail: chezhao@nus.edu.sg

Experimental Details

Details of Material Preparation

Preparation of ZIF-8 nanoparticles, NaCl/ZIF-8 composite and the MOF-derived carbon network (MCN): ZIF-8 nanocrystals were prepared according to the previous study.[1] Briefly, zinc nitrate tetrahydrate (0.261 g, 1 mmol) and 2-methylimidazaole (0.657 g, 8 mmol) were dissolved in 20 mL of methanol, respectively, and then mixed and stirred for 24 hours. The product was collected by 10,000 rpm centrifuge and washed with pure methanol for 3 times. NaCl/ZIF-8 composites were prepared by dispersing ZIF-8 (0.1 g) and NaCl (2.0 g) in a mixed solvent containing methanol (1 mL) and water (9 mL), and collected by vacuum drying. For MOF-derived carbon network (MCN), NaCl/ZIF-8 composite (2.1 g) was pyrolyzed at 900 °C under N_2 atmosphere for 3 hours. The product was collected and soaked in deionized water (DIW, 20 mL) at 80 °C overnight to remove NaCl, washed with DIW, collected by filtration, and dried under vacuum for further usage.

Preparation of NiFe layered double hydroxide (LDH), MCN-LDH composites and MCN/LDH physical mixture: LDH nanoplates were prepared based on a previous study.[2] Briefly, nickel nitrate hexahydrate aqueous solution (0.857 mL, 0.5 M), ferric chloride hexahydrate aqueous solution (0.143 mL, 0.5 M), urea aqueous solution (2 mL, 5 M), and DIW (7 mL) were mixed and stirred in a Teflon liner. The Teflon liner was then put into an autoclave and heated at 120 °C for 12 hours. The orange precipitate was collected by 4,000 rpm centrifuge and washed with DIW for 3 times. The preparation of MCN-LDH composites was similar, except that 10 mg of CN was added to give a loading of MCN-LDH-1.0. For MCN-LDH-0.3 to MCN-LDH-2.0, the initial feed of Ni and Fe was proportionally adjusted from 30 % to 200 % of the above volume, while the added volume of DIW was adjusted as well to keep a total volume of 10 mL. The MCN/LDH-1.5 mixture was physically mixed and ball-milled for 15 minutes. The weight ratio between MCN and LDH in the mixture was the same as that of MCN-LDH-1.5, which was determined by inductively coupled plasma optical emission spectrometry (ICP-OES).

Details of Material Characterization

Field-emission scanning electron microscopy (SEM) was conducted on a JEOL JSM-7610F scanning electron microscope (5 kV). Field-emission transmission electron microscopy (TEM) was conducted on a JEOL-TEM 2010F transmission electron microscope (200 kV). Powder X-ray diffraction (PXRD) patterns were collected on a Rigaku MiniFlex 600 equipped with a Cu sealed tube (λ = 1.54178 Å) at a scan rate of 4 ° min^{-1}. Raman spectra were collected on a Horiba Modular Raman system using a 50 x objective and a 514.5 nm laser source. Inductively coupled plasma optical emission spectrometry (ICP-OES) was performed on a Thermo Scientific iCAP 6000 ICP emission spectrometer. Each sample (20 mg) was soaked in HNO_3 (0.5 M, 10 mL) overnight, and the supernatant (1 mL) was diluted into 10 mL with DIW for measurement. Atomic force microscopy data were collected on a Bruker Dimension Icon atomic force microscope. Samples were deposited on silicon wafers and tested using tapping mode.

N_2 sorption isotherms were measured up to 1 bar using a Quantachrome Instruments Autosorb-iQ surface area and pore size analyzer. Before each measurement, the sample (~ 50 mg) was degassed under reduced pressure (< 10^{-2} Pa) at 150 °C for 12 h. UHP grade N_2 and He were used for all the measurements. The temperature of 77 K was maintained with a liquid nitrogen bath. Pore size distribution data were calculated from the N_2 sorption isotherms based on quenched solid density functional theory (QSDFT) model in the Autosorb-iQ software package (assuming slit/cylinder geometry).

X-ray photoelectron spectroscopy (XPS) spectra were collected on a Kratos AXIS Ultra DLD surface analysis instrument using a monochromatic Al Kα radiation (1486.71 eV) at 15 kV as the excitation source. The takeoff angle of the emitted photoelectrons was 90 ° (the angle between the plane of sample surface and the entrance lens of the detector). Peak position was corrected by referencing the C 1s peak position of adventitious carbon for a sample (284.6 eV), and shifting all other peaks in the spectrum accordingly. Fitting was done using the program CasaXPS. Each relevant spectrum was fit to a Shirley type background to correct for the rising edge of backscattered electrons that shifts the baseline higher at high binding energies. Peaks were fit as asymmetric

Gaussian/Lorentzians, with 0-30 % Lorentzian character. The FWHM of all sub-peaks was constrained to 0.7-2 eV, as dictated by instrumental parameters, lifetime broadening factors, and broadening due to sample charging. With this native resolution set, peaks were added, and the best fit, using a least-squares fitting routine, was obtained while adhering to the constraints mentioned above.

X-ray absorption spectra at the Ni K-edge were collected at Advanced Photon Source of Argonne National Laboratory, U.S.A. The Co K-edge X-ray absorption near edge structure (XANES) data were recorded in a transmission mode at sector 12 BM and 20 BM. The acquired extended X-ray absorption fine structure (EXAFS) data were extracted and processed according to the standard procedures using the ATHENA module implemented in the IFEFFIT software packages. The k^3-weighted EXAFS spectra were obtained by subtracting the post-edge background from the overall absorption and then normalizing with respect to the edge-jump step. Subsequently, k^3-weighted $\chi(k)$ data in the k-space were Fourier transformed to real (R) space using a hanning windows (dK = 1.0 $Å^{-1}$) to separate the EXAFS contributions from different coordination shells.

Details of Electrochemical Experiments

Electrochemical properties of the obtained samples were studied using a PINE rotating ring-disk electrode setup (AFMSRCE, PINE Research) and an electrochemical workstation (760E, CH Instruments). The catalyst (5 mg) was dispersed in 1 mL of solution containing DIW (0.4 mL), ethanol (0.58 mL) and 5 wt% Nafion solution (0.02 mL). The dispersion was sonicated for 1 hour before use. For each measurement, 20 μL of ink was pipetted onto the working electrode (AFE7R9GCPT, PINE Research), resulting in a catalyst loading of ca. 0.4 mg cm^{-2}. The loading of noble metal catalyst benchmark Pt/C-RuO_2 is 0.04 mg_{Pt} cm^{-2} and 0.04 mg_{IrO2} cm^{-2}.The Pt/C-RuO_2 is prepared by sonicating 20% Pt/C (250 mg, 35849, Alfa Aesar) and RuO_2 (50 mg, 238058, Sigma Aldrich) in ethanol (10 mL). The mixture dispersion is vacuum dried at 80 °C overnight to collect the Pt/C-RuO_2 powder. The electrolyte was bubbled with Ar or O_2 for at least 30 min before each measurement.

A. Cyclic voltammetry (CV)

CV data was collected by using cyclic sweep from 0.2 V to -0.8 V (vs Ag/AgCl in 3 M KCl, same below) at a scan rate of 20 mV s^{-1}. The catalyst was at least cycled for 50 times before data collection.

B. ORR catalytic activity

ORR catalytic activity was investigated using rotating ring-disk electrode (RRDE) at a rotation speed of 1600 rpm. Capacitive background current was first recorded in the Ar-purged electrolyte using cathodic linear sweep voltammetry (CLSV) from 0.2 V to -0.8 V at a scan rate of 10 mV s^{-1}. The electrolyte was subsequently purged with O_2, followed by CLSV at the same scan rate for ORR activity test. The oxygen reduction current was corrected by subtracting the background current from the CLSV obtained in O_2-saturated electrolyte.

C. Rotating disk electrode (RDE) measurements

For RDE measurements, catalysts were scanned cathodically from 0.2 V to -0.8 V at a scan rate of 10 mV s^{-1} with varying rotation speed from 400 rpm to 2500 rpm. Koutecky–Levich plots were derived from RDE measurement results to calculate the number of electrons transferred based on the following Koutecky-Levich equation:

$$\frac{1}{j} = \frac{1}{j_L} + \frac{1}{j_K} = \frac{1}{B\omega^{1/2}} + \frac{1}{j_K}$$
$$B = 0.2nFC_0(D_0)^{2/3}\nu^{-1/6}$$

where j is the measured current density, j_K and j_L are the kinetic- and diffusion-limiting current densities, respectively, ω is the angular velocity, n is transferred electron number, F is the Faraday constant, C_0 is the bulk concentration of O_2, D_0 is the diffusion coefficient of O_2 in electrolyte and v is the kinematic viscosity of the electrolyte.

D. Rotating ring-disk electrode (RRDE) measurements

For the RRDE measurements, the ring potential was kept constant at 1.5 V vs RHE. The HO_2^- yield (%) and electron transfer number (n) were determined by the following equations

$$HO_2^-(\%) = 200 \times \frac{I_r \times N}{I_d + I_r / N} \qquad n = 4 \times \frac{I_d}{I_d + I_r / N}$$

where I_d is disk current, I_r is ring current and N is current collection efficiency of the Pt ring [40%, corrected by $Fe(CN)_6^{3-}/Fe(CN)_6^{4-}$].

E. Accelerated degradation tests (ADTs)

ORR activity was firstly measured by RDE measurement. Subsequently, the catalyst was cycled from 0 V to - 0.4 V for 10,000 cycles in O_2-saturated electrolyte at a scan rate of 50 mV s^{-1}. The electrode rotation speed was 400 rpm. After cycling, ORR activity of the cycled catalyst was measured again. OER activity was firstly measured by RDE measurement. Subsequently, the catalyst was linearly scanned from 0 V to 1.0 V for 1,000 times in O_2-saturated electrolyte at a scan rate of 10 mV s^{-1}. The electrode rotation speed was 1600 rpm. After cycling, OER activity of the cycled catalyst was measured again.

F. Electrochemical impedance spectroscopy (EIS)

For the collection of OER-EIS spectra, the initial potential was set at a value which was 0.05 V higher than the OER onset potential. The amplitude was 0.005 V and the frequency was from 0.05 Hz to 100k Hz.

Details of Rechargeable Zn-Air Battery Tests

The catalyst (12 mg) was dispersed in ethanol (6 mL) and sonicated for 1 hour. The slurry was brushed onto a piece of 2 cm x 2 cm carbon paper (10 BC, SGL Carbon) and dried naturally. The carbon paper has a catalyst loading of 3 mg cm^{-2}. The loading of 20% Pt/C is 0.3 mg_{Pt} cm^{-2}. A zinc plate was used as anode and the assembly was tested in ambient air atmosphere. The battery contains 25 mL of aqueous electrolyte (6 M KOH and 0.2 M $ZnCl_2$). Catalyst durability was evaluated by continuous cycling of discharging and charging the batteries at a fixed current density of 10 mA cm^{-2} for 7500 minutes.

Details of Computational Study on OER Mechanism

The computational study on OER mechanism was performed using the Dmol^3 package of Accelrys Materials Studio 2016 (Version 16.1.0.21). The exchange-correlation functional used is the Perdew-Burke-Ernzerhof of generalized gradient approximation (GGA-PBE). A 3x2 super cell with 180

atoms was used to simulate the structure of LDH. Considering the relativity effect, the density functional semi-core pseudopotential method was employed for the Ni and Fe atoms, whereas the P, H, and O atoms were dealt with an all-electron basis set. The valence electron functions were expanded into a set of numerical atomic orbitals with a double numerical basis with polarization (DNP) functions. The structure optimization is based on the following points: (1) an energy tolerance of 2.0×10^{-5} Ha per atom; (2) a maximum force tolerance of 4.0×10^{-3} Ha $Å^{-1}$; and (3) a maximum displacement tolerance of 5.0×10^{-3} Å.

At alkaline environment, the OER proceeds in four electrons steps and can be written as follows:

$$* + OH^- \rightarrow OH * + e^- \quad (1)$$

$$OH* + OH^- \rightarrow O* + H_2O + e^- \quad (2)$$

$$O* + OH^- \rightarrow OOH* + e^- \quad (3)$$

$$OOH* + OH^- \rightarrow O_2* + H_2O + e^- \quad (4)$$

where * presents an adsorption site on the catalyst, and OH*, O*, and OOH* denotes the corresponding absorbed intermediates. Then, at standard conditions, the free energy change for all OER electrochemical steps (ΔG1-4) can be expressed as:

$$\Delta G_1 = \Delta G_{OH*}$$

$$\Delta G2 = \Delta G_{O*} - \Delta G_{OH*}$$

$$\Delta G_3 = \Delta G_{OOH*} - \Delta G_{O*}$$

$$\Delta G_4 = 4.92 - \Delta G_{OOH*}$$

In detail, the reaction free energy for adsorbates (ΔG_{ads}) was calculated according to the following formula:

$$\Delta G_{ads} = \Delta E_{ads} + \Delta E_{ZPE} - T\Delta S$$

where E_{ZPE} is the zero-point energy, ΔS is the entropy change, and T is the system temperature (298.15 K, in our work). The binding energy (ΔE_{ads}) for OOH*, O*, and OH* could be calculated by the following equation:

$$\Delta E_{OH*} = E_{OH*} - E_{*} - (E_{H2O} - 1/2\ E_{H2})$$

$$\Delta E_{O*} = E_{O*} - E_{*} - (E_{H2O} - E_{H2})$$

$$\Delta E_{OOH*} = E_{OOH*} - E_{*} - (2\ E_{H2O} - 3/2\ E_{H2})$$

where E_{OOH*}, E_{O*}, E_{OH*} and E* represent the calculated DFT total energy of the pristine substrate and those absorbed with OOH*, O*, and OH*, respectively, and E_{H2O} and E_{H2} are the total energy of H_2O and H_2 molecules in the gas phase, respectively.

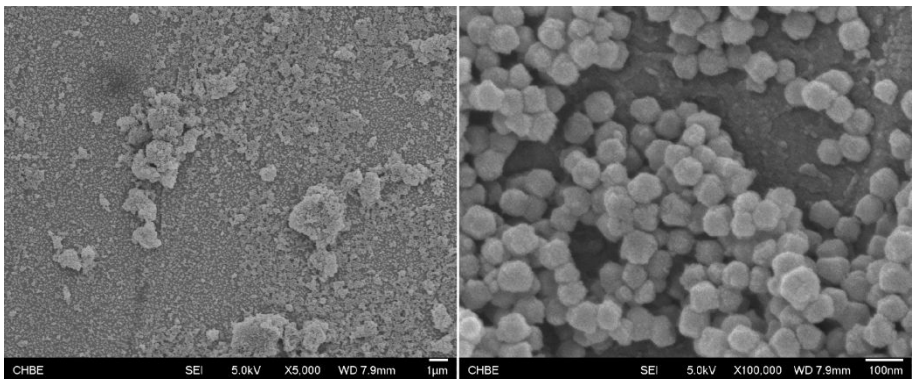

Figure S1. SEM images of pristine ZIF-8 nanocrystals.

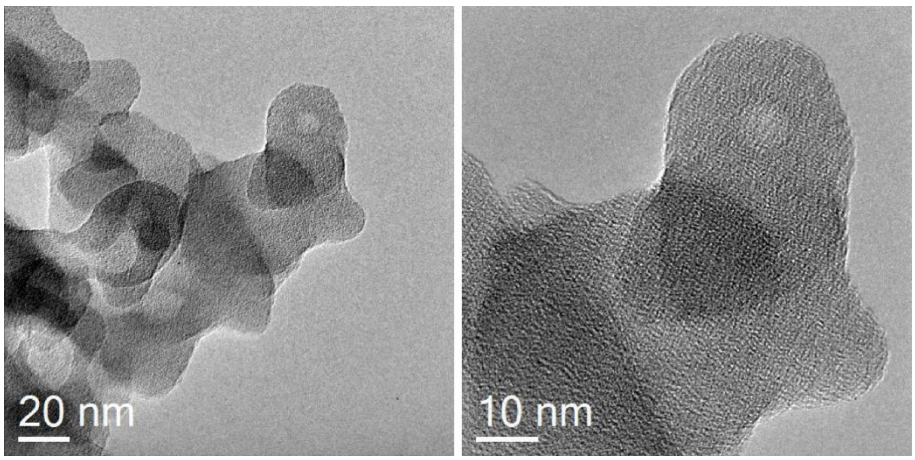

Figure S2. TEM images of carbon material derived from conventional pyrolysis of ZIF-8.

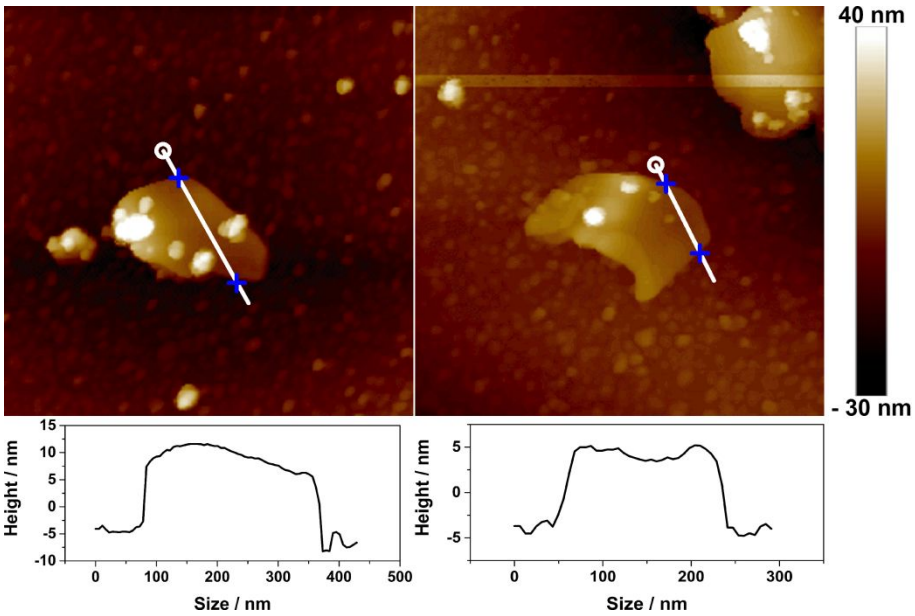

Figure S3. AFM images of NiFe LDH nanoplates.

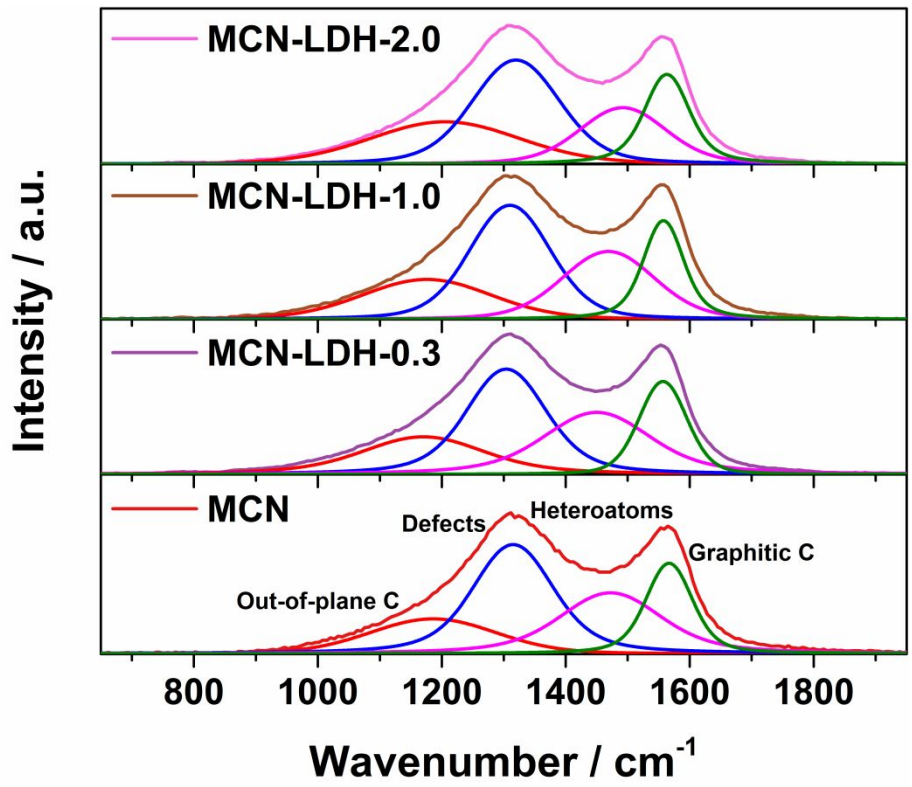

Figure S4. Raman spectra of MCN, MCN-LDH-0.3, MCN-LDH-1.0, and MCN-LDH-2.0, showing the signals originated from the carbon network.

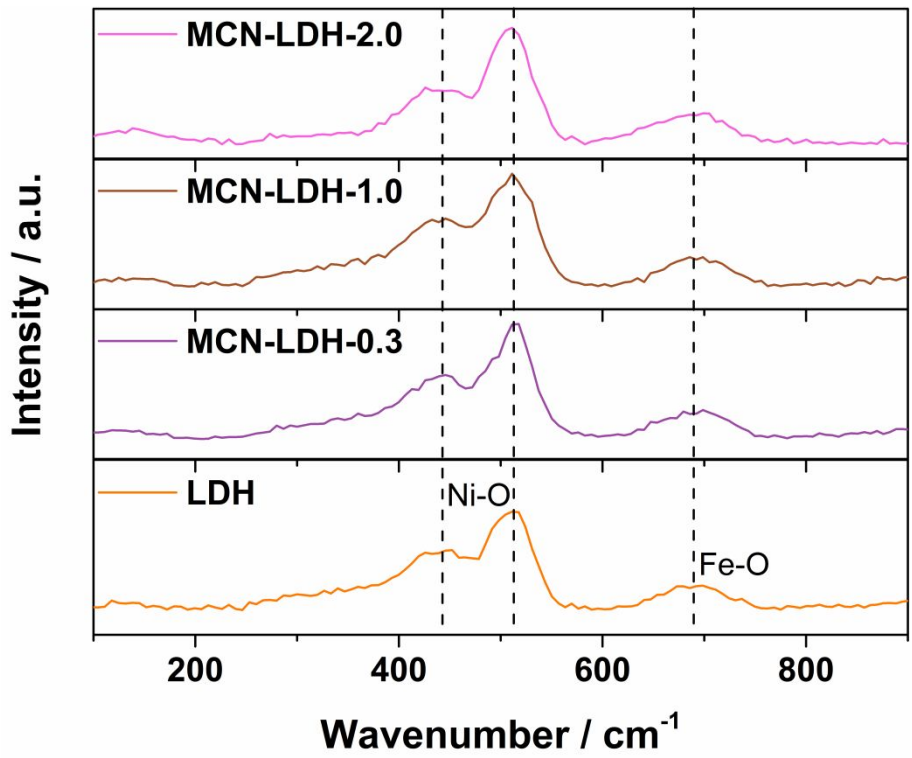

Figure S5. Raman spectra of MCN, MCN-LDH-0.3, MCN-LDH-1.0, and MCN-LDH-2.0, showing the signals originated from the LDH nanoplates.

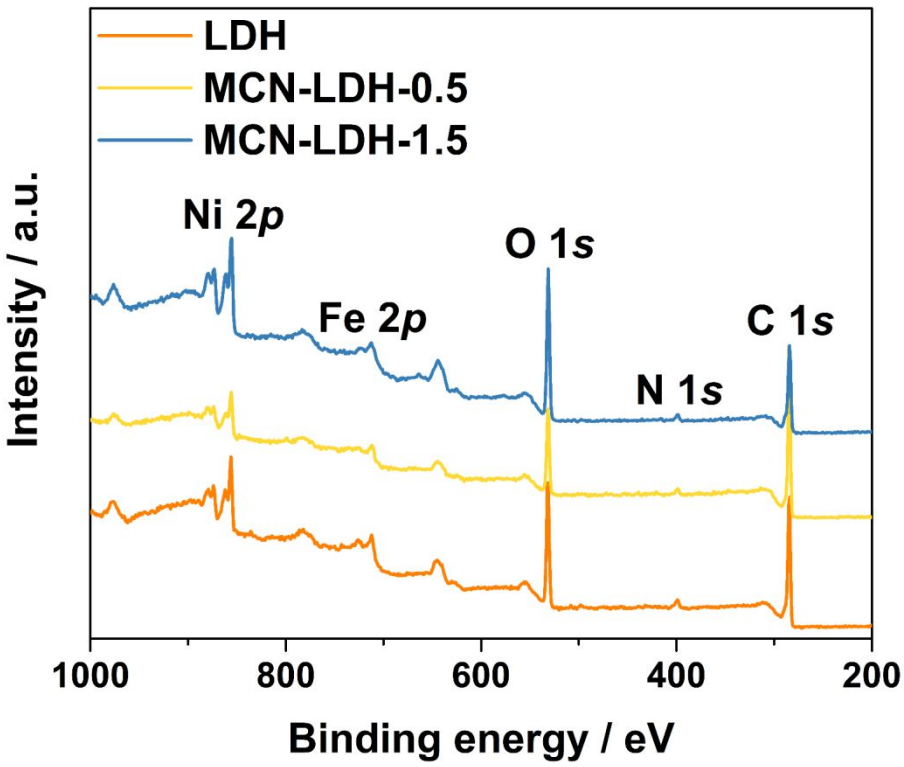

Figure S6. Full XPS spectra of LDH, MCN-LDH-0.5, and MCN-LDH-1.5.

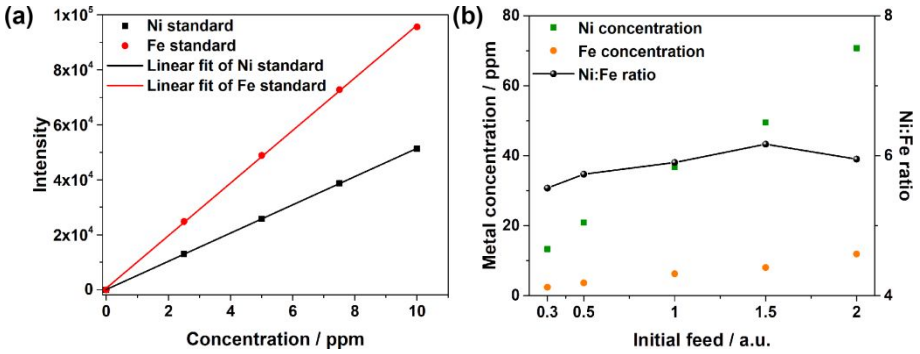

Figure S7. (a) Calibration curves for Ni and Fe in the ICP-OES analysis; (b) LDH loadings and ratios of Ni to Fe in MCN-LDH composites determined by ICP.

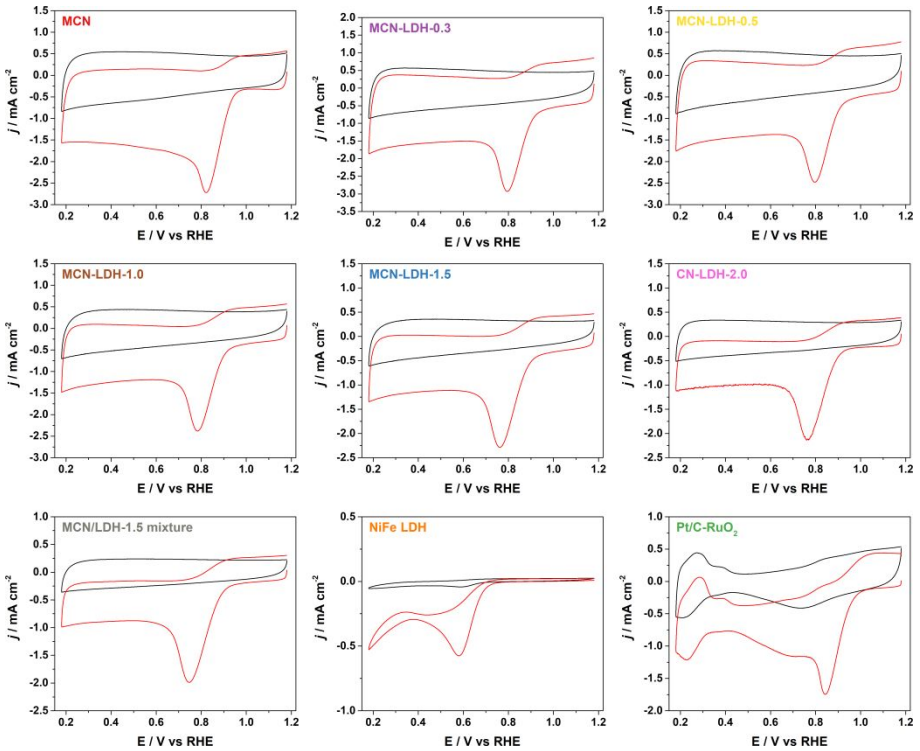

Figure S8. CV voltammograms of MCN, LDH and MCN-LDH composites in N_2- (black) and O_2- (red) saturated electrolyte.

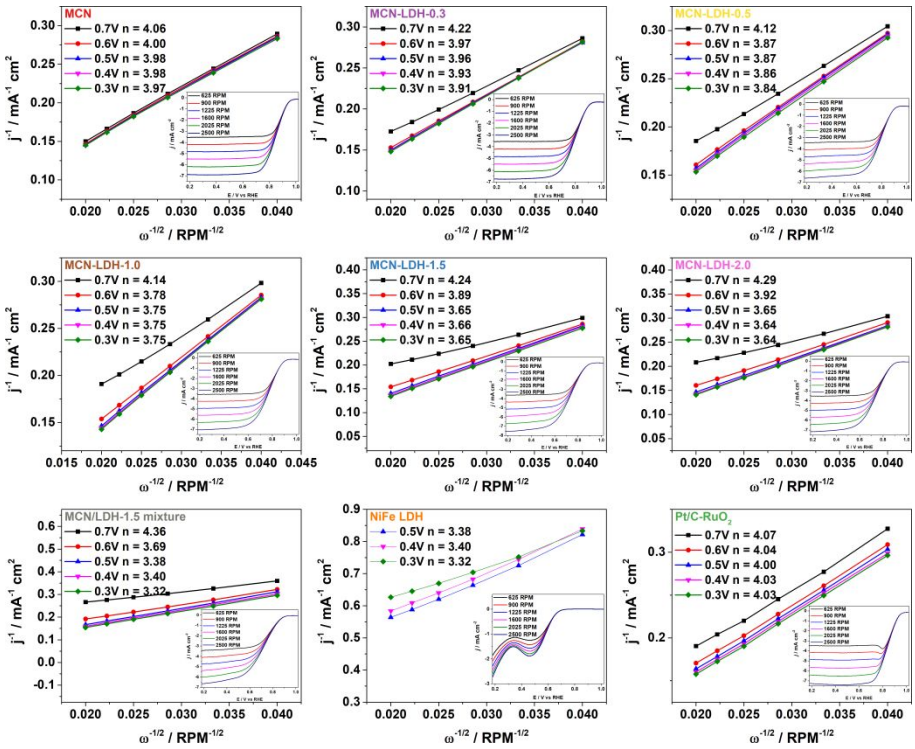

Figure S9. Number of electrons transferred and peroxide yield of MCN and MCN-LDH composites during ORR catalysis determined by Koutecky-Levich equations.

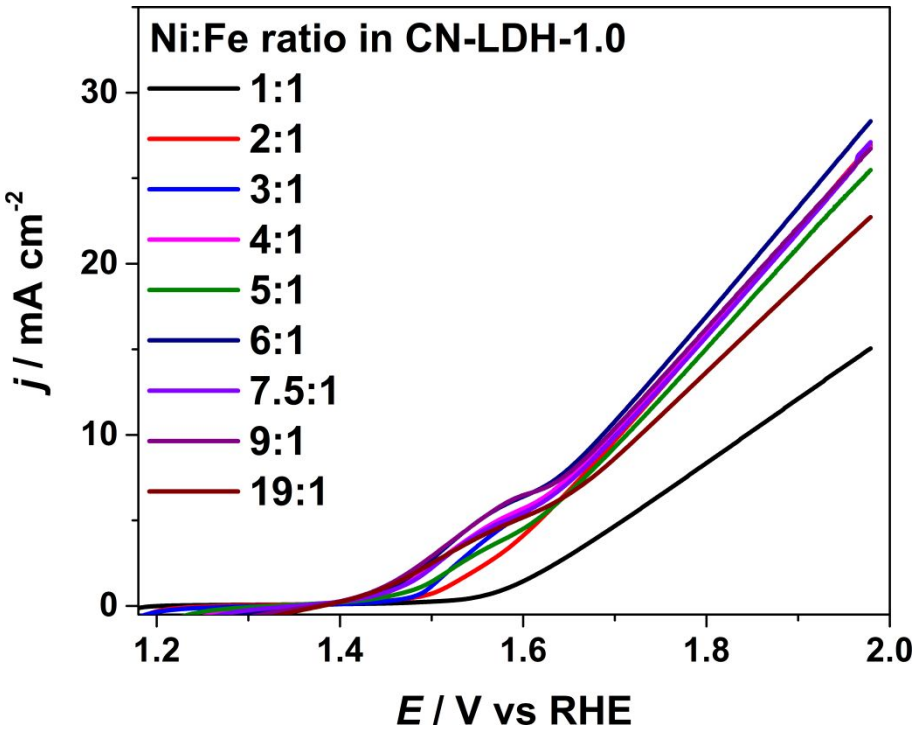

Figure S10. The effect of the ratio of Ni to Fe in MCN-LDH composites on the OER catalytic activity. The ratio of Ni to Fe was varied from 1:1 to 19:1 and the MCN-LDH-1.0 (Ni:Fe = 6:1) showed the highest OER current density.

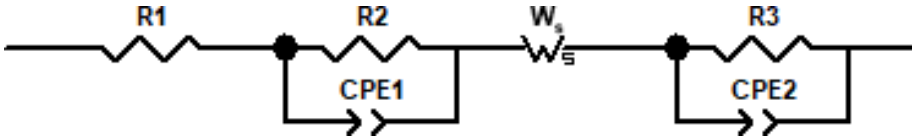

Figure S11. Equivalent circuit model for fitting the EIS spectra of CN-LDH composites, where R1 is electrolyte resistance, R2 is Nafion layer resistance, Ws is diffusional resistance, and R3 is electron transfer resistance.

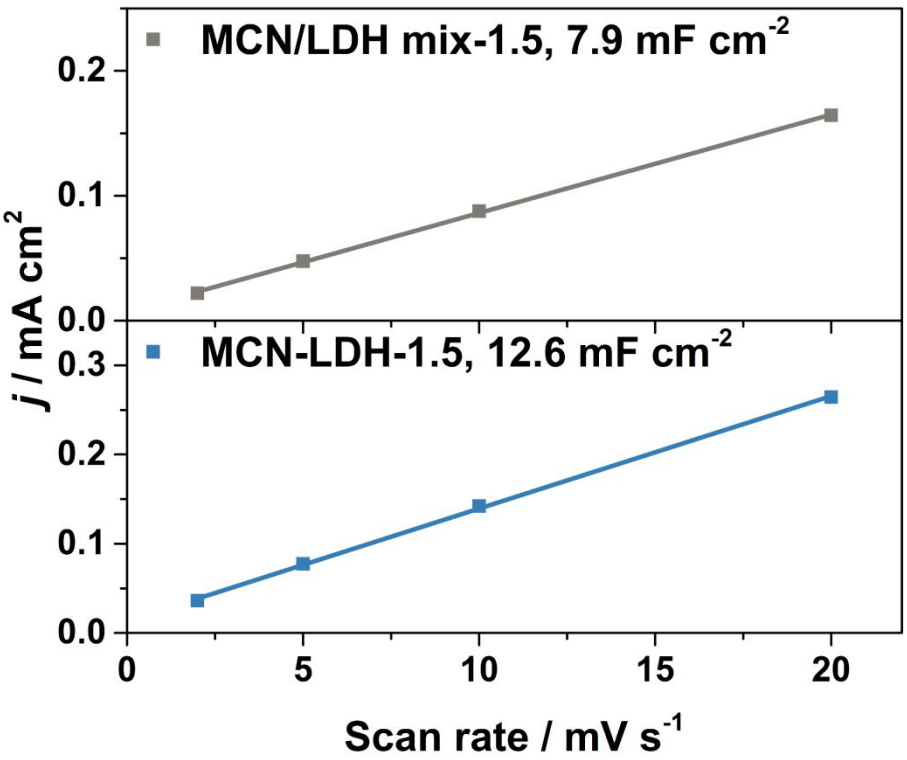

Figure S12. Double-layer capacitance of MCN-LDH-1.5 composite and the physical mixture control group.

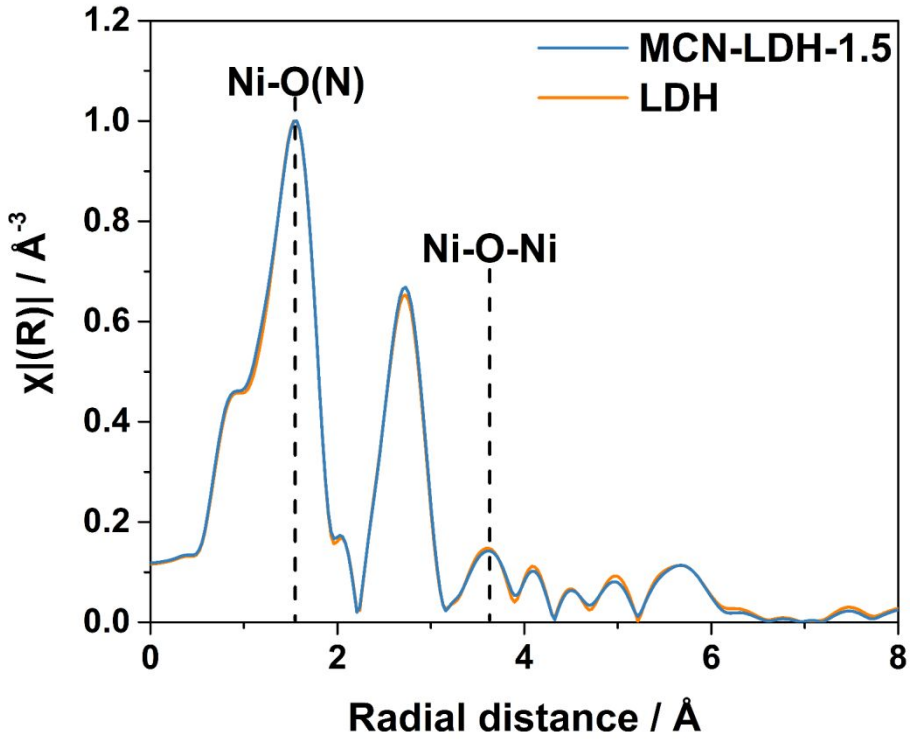

Figure S13. k^3-weighted Fourier transformed extended X-ray absorption spectra of MCN/LDH-1.5 physical mixture and MCN-LDH-1.5 composite.

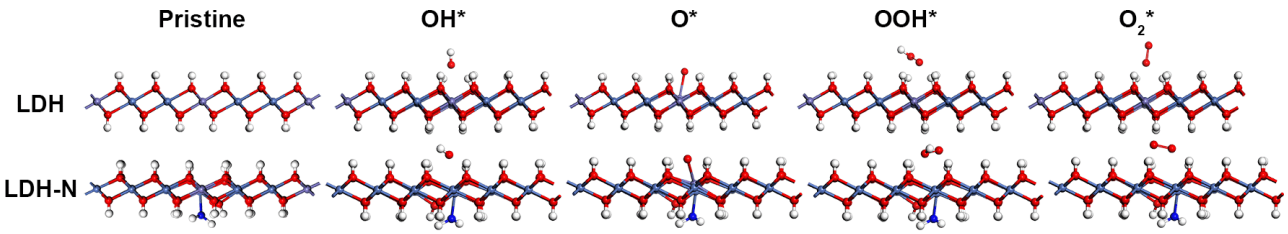

Figure S14. Geometrically optimized structures of pristine and intermediate-adsorbed LDH and LDH with additional Ni-N bonds.

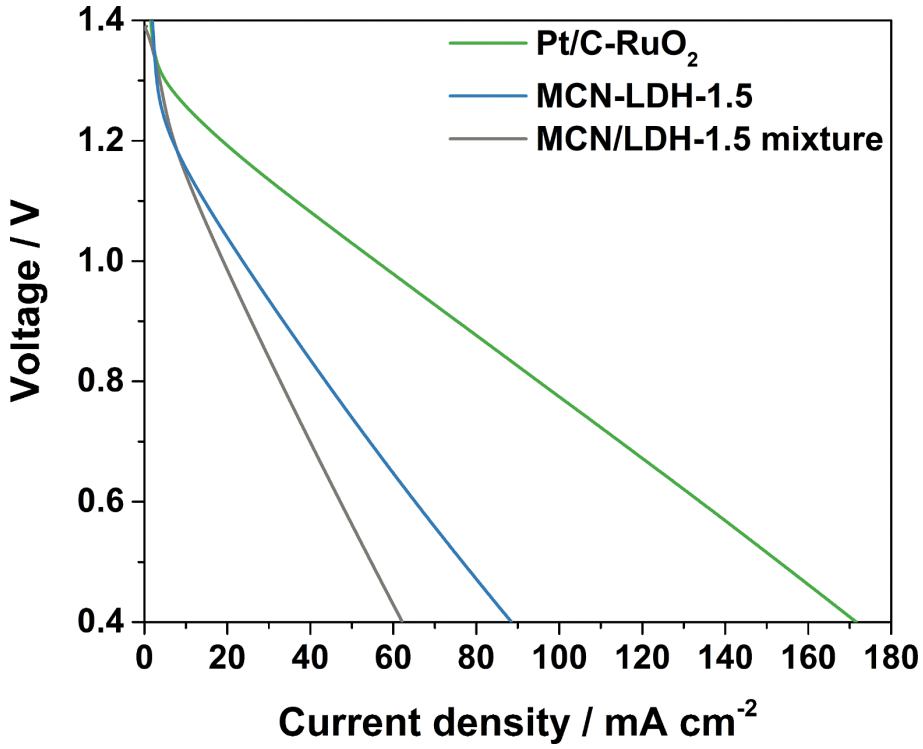

Figure S15. LSVs of batteries using Pt/C-RuO_2, MCN-LDH-1.5, and MCN/LDH-1.5 mixture in the air cathodes.

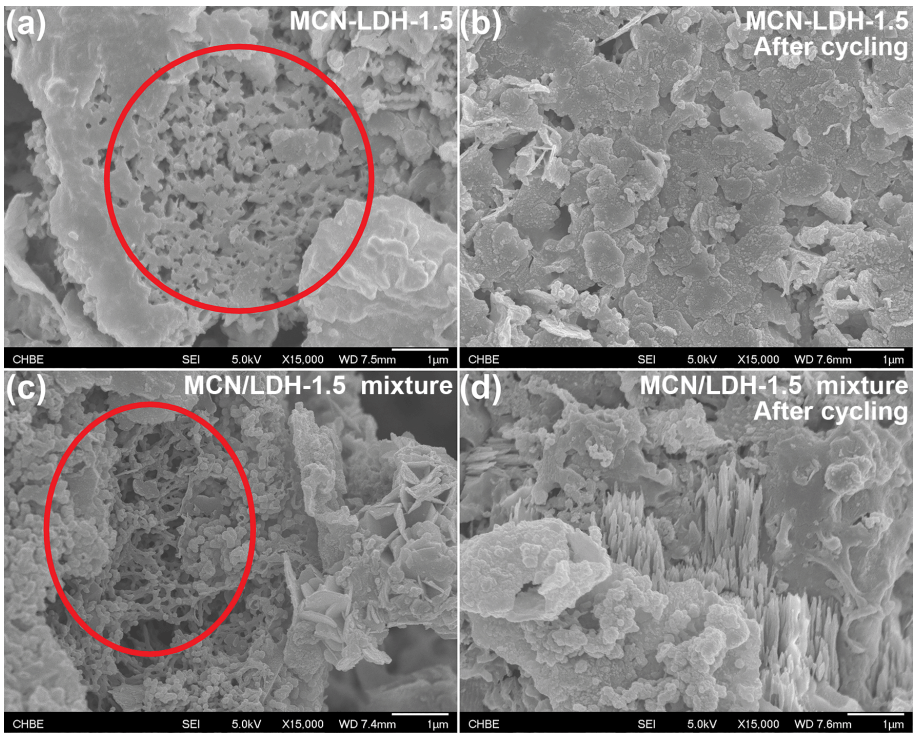

Figure S16. SEM images of air electrodes containing MCN-LDH-1.5 and MCN/LDH-1.5 physical mixture: (a, c) before discharge/recharge cycling; (b, d) after discharge/recharge cycling.

Table S1. Deconvolution results of carbon Raman signal of MCN and CN-LDH composites.

	Out-of-plane C / rel. %	D / rel. %	Heteroatoms / rel. %	G / rel. %	D/G
CN	16.91	38.05	26.89	18.15	2.10
CN-LDH-0.3	19.33	35.21	27.86	17.60	2.00
CN-LDH-1.0	20.09	37.28	25.01	17.62	2.12
CN-LDH-2.0	19.67	36.45	26.04	17.83	2.04

Table S2. Deconvolution results of N 1s XPS spectra of CN and CN-LDH composites.

	Pyridine N / rel. %	Pyrrolic N / rel. %	Graphitic N / rel. %	Oxidized N / rel. %
CN	23.44	18.89	37.38	20.28
CN-LDH-0.5	23.88	16.76	39.04	20.32
CN-LDH-1.5	25.70	16.32	37.23	20.75

Table S3. BET surface area, ORR activity, and OER activity of CN, LDH, and CN-LDH composites.

	B.E.T. surface area / $m^2\ g^{-1}$	ORR activity[a]			OER activity[a]	
		E_{onset}[b] / V	$E_{half\text{-}wave}$[c] / V	j_{max}[d] / mA cm^{-2}	*E @ j = 10 mA cm^{-2}*	j_{max}[e] / mA cm^{-2}
CN	1177	0.965	0.861	5.348	/	1.49
CN-LDH-0.3	983	0.962	0.838	5.293	1.801	17.63
CN-LDH-0.5	702	0.964	0.843	5.448	1.710	28.62
CN-LDH-1.0	620	0.960	0.827	5.402	1.689	30.56
CN-LDH-1.5	548	0.958	0.826	5.388	1.670	33.98
CN-LDH-2.0	505	0.956	0.814	5.366	1.687	29.59
NiFe LDH	164	0.674	/	/	1.719	21.41
Pt/C-RuO_2	/	0.970	0.834	5.645	1.808	20.55
CN/LDH-1.5 mixture	/	0.901	0.729	5.322	1.809	20.96

[a] In 0.1M KOH; [b] Determined when j = 0.1 mA cm^{-2}; [c] The potential when $j = ½\ j_{max}$; [d] E = 0.18 V vs RHE; [e] E = 1.98 V vs RHE.

Table S4. Equivalent circuit fitting results of CN and CN-LDH composites.

	R1 (Ω)	R2 (Ω)	Ws (Ω)	R3 (Ω)
CN-LDH-0.3	12.67	30.72	12.23	513.6
CN-LDH-0.5	13.81	27.15	14.19	405.9
CN-LDH-1.0	11.75	30.02	11.546	455.5
CN-LDH-1.5	13.91	27.53	16.26	327.8
CN-LDH-2.0	12.21	29.44	10.706	440.4
NiFe LDH	12.19	33.12	7.878	619.5
CN/LDH-1.5 mixture	11.94	29.95	12.07	587.2

Table S5. The Gibbs free energies of the elementary steps of OER on the proposed models of LDH and LDH with additional Ni-N coordination bonds.

	ΔG_1 / eV	ΔG_2 / eV	ΔG_3 / eV	ΔG_4 / eV
LDH	0.96	2.79	0.42	0.75
LDH with additional Ni-N bonds	1.15	2.05	0.91	0.81

Table S6. Summary of recently published composite electrocatalysts for ORR-OER bifunctional catalysis.

Sample name	Durability (discharge/recharge) test condition	Discharge voltage / V	Recharge voltage / V	Round-trip voltage / V	Reference
MCN-LDH	10 mA cm^{-2}, 120 hours.	1.08	2.02	0.94	This work
$Fe_{0.5}Co_{0.5}O_x$/NrGO	10 mA cm^{-2}, 120 hours.	/	/	0.89	[3]
Ni-MnO/rGO	10 mA cm^{-2}, 35 hours.	/	/	0.98	[4]
$ZnCo_2O_4$/N-CNT	Discharge at 10 mA cm^{-2} and recharge at 100 mA cm^{-2}, 6 hours.	1.35	2.19	0.84	[5]
CoS_x@PCN/rGO	15 mA cm^{-2}, 44 hours.	~0.7	~2.0	1.3	[6]
S-GNS/$NiCo_2S_4$	10 mA cm^{-2}, 100 hours.	1.19	1.89	0.70	[7]
$CuCo_2O_4$/N-CNT	20 mA cm^{-2}, 40 hours.	1.14	1.53	0.39	[8]
S,N-Fe/N/C-CNT	5 mA cm^{-2}, duration not mentioned.	~1.1	2.0	0.9	[9]
FeNi-NC	8 mA cm^{-2}, 25 hours.	1.20	2.02	0.82	[10]
3D NCNT array	5 mA cm^{-2}, 3 hours.	1.02	1.98	0.96	[11]
$NiCo_2S_4$/N-CNT	10 mA cm^{-2}, 20 hours.	1.35	1.98	0.63	[12]
$MnCo_2O_4$/NMCNA	10 mA cm^{-2}, 35 hours.	/	/	~0.8	[13]
CFZr(0.3)/N-rGO	15 mA cm^{-2}, 10 hours.	~1.0	2.05	1.05	[14]
Ni_3FeN/NRGO	10 mA cm^{-2}, 30 hours.	1.12	1.94	0.82	[15]

References

1. Cravillon, J.; Münzer, S.; Lohmeier, S.-J.; Feldhoff, A.; Huber, K.; Wiebcke, M., Rapid Room-Temperature Synthesis and Characterization of Nanocrystals of a Prototypical Zeolitic Imidazolate Framework. *Chem. Mater.* **2009,** *21*, 1410-1412.
2. Lu, Z.; Xu, W.; Zhu, W.; Yang, Q.; Lei, X.; Liu, J.; Li, Y.; Sun, X.; Duan, X., Three-Dimensional NiFe Layered Double Hydroxide Film for High-Efficiency Oxygen Evolution Reaction. *Chem. Commun.* **2014,** *50*, 6479-6482.
3. Wei, L.; Karahan, H. E.; Zhai, S.; Liu, H.; Chen, X.; Zhou, Z.; Lei, Y.; Liu, Z.; Chen, Y., Amorphous Bimetallic Oxide-Graphene Hybrids as Bifunctional Oxygen Electrocatalysts for Rechargeable Zn-Air Batteries. *Adv. Mater.* **2017,** *29*, 1701410.
4. Fu, G.; Yan, X.; Chen, Y.; Xu, L.; Sun, D.; Lee, J. M.; Tang, Y., Boosting Bifunctional Oxygen Electrocatalysis with 3D Graphene Aerogel-Supported Ni/MnO Particles. *Adv. Mater.* **2018,** *30*, 1704609.
5. Liu, Z. Q.; Cheng, H.; Li, N.; Ma, T. Y.; Su, Y. Z., $ZnCo_2O_4$ Quantum Dots Anchored on Nitrogen-Doped Carbon Nanotubes as Reversible Oxygen Reduction/Evolution Electrocatalysts. *Adv. Mater.* **2016,** *28*, 3777-84.
6. Niu, W.; Li, Z.; Marcus, K.; Zhou, L.; Li, Y.; Ye, R.; Liang, K.; Yang, Y., Surface-Modified Porous Carbon Nitride Composites as Highly Efficient Electrocatalyst for Zn-Air Batteries. *Adv. Energy Mater.* **2018,** *8*, 1701642.
7. Liu, W.; Zhang, J.; Bai, Z.; Jiang, G.; Li, M.; Feng, K.; Yang, L.; Ding, Y.; Yu, T.; Chen, Z.; Yu, A., Controllable Urchin-Like $NiCo_2S_4$ Microsphere Synergized with Sulfur-Doped Graphene as Bifunctional Catalyst for Superior Rechargeable Zn-Air Battery. *Adv. Funct. Mater.* **2018,** *28*, 1706675.
8. Cheng, H.; Li, M.-L.; Su, C.-Y.; Li, N.; Liu, Z.-Q., Cu-Co Bimetallic Oxide Quantum Dot Decorated Nitrogen-Doped Carbon Nanotubes: A High-Efficiency Bifunctional Oxygen Electrode for Zn-Air Batteries. *Adv. Funct. Mater.* **2017,** *27*, 1701833.
9. Chen, P.; Zhou, T.; Xing, L.; Xu, K.; Tong, Y.; Xie, H.; Zhang, L.; Yan, W.; Chu, W.; Wu, C.; Xie, Y., Atomically Dispersed Iron-Nitrogen Species as Electrocatalysts for Bifunctional Oxygen Evolution and Reduction Reactions. *Angew. Chem. Int. Ed.* **2017,** *56*, 610-614.
10. Yang, L.; Zeng, X.; Wang, D.; Cao, D., Biomass-derived FeNi alloy and nitrogen-codoped porous carbons as highly efficient oxygen reduction and evolution bifunctional electrocatalysts for rechargeable Zn-air battery. *Energy Storage Mater.* **2018,** *12*, 277-283.

11. Li, Z.; Shao, M.; Yang, Q.; Tang, Y.; Wei, M.; Evans, D. G.; Duan, X., Directed synthesis of carbon nanotube arrays based on layered double hydroxides toward highly-efficient bifunctional oxygen electrocatalysis. *Nano Energy* **2017,** *37*, 98-107.
12. Han, X.; Wu, X.; Zhong, C.; Deng, Y.; Zhao, N.; Hu, W., $NiCo_2S_4$ nanocrystals anchored on nitrogen-doped carbon nanotubes as a highly efficient bifunctional electrocatalyst for rechargeable zinc-air batteries. *Nano Energy* **2017,** *31*, 541-550.
13. Bin, D.; Guo, Z.; Tamirat, A. G.; Ma, Y.; Wang, Y.; Xia, Y., Crab-shell induced synthesis of ordered macroporous carbon nanofiber arrays coupled with $MnCo_2O_4$ nanoparticles as bifunctional oxygen catalysts for rechargeable Zn-air batteries. *Nanoscale* **2017,** *9*, 11148-11157.
14. Kashyap, V.; Kurungot, S., Zirconium-Substituted Cobalt Ferrite Nanoparticle Supported N-doped Reduced Graphene Oxide as an Efficient Bifunctional Electrocatalyst for Rechargeable Zn–Air Battery. *ACS Catal.* **2018,** *8*, 3715-3726.
15. Fan, Y.; Ida, S.; Staykov, A.; Akbay, T.; Hagiwara, H.; Matsuda, J.; Kaneko, K.; Ishihara, T., Ni-Fe Nitride Nanoplates on Nitrogen-Doped Graphene as a Synergistic Catalyst for Reversible Oxygen Evolution Reaction and Rechargeable Zn-Air Battery. *Small* **2017,** *13*.